

Improved Isolation Metamaterial Inspired mm-Wave MIMO Dielectric Resonator Antenna for 5G Application

Nimmagadda S. Murthy*

Abstract—A rectangular Dielectric Resonator Antenna (DRA) four element Multiple in Multiple Out (MIMO) is proposed for 5G application, and each element is supplied with slot-coupled microstrip feed. The entire construction has a dimension of $20\text{ mm} \times 40\text{ mm}$. Four Dielectric Resonators are mounted exactly above the slot. In order to improve the isolation, metamaterial is printed on top of the dielectric resonators, which move away the solidest coupling fields. As the metamaterial structure interacts with electromagnetic fields, field distributions are disturbed which results in reduction of coupled fields. Since the metamaterials are printed on top of the dielectric resonator, the proposed antenna structure has the simplest and compact design. The proposed structure is operating with an impedance bandwidth of 2.23 GHz with operating range from 26.71 GHz to 28.91 GHz, which covers the 28 GHz (27.5 GHz–28.35 GHz) band allotted by Federal Communications Commission (FCC) for 5G application. With all four-port excitation, the proposed structure shows a broadside radiation pattern with gain above 7 dBi in the entire operating bands. The Envelope Correlation Coefficient (ECC) for operating bands is within the target value. They are designed and fabricated to validate the proposed antenna. The simulated and measured values are nearly equal, which means that the proposed MIMO DRA is the right choice for mm-Wave 5G implementation.

1. INTRODUCTION

With the extraordinary development of Internet of Things (IoT), virtual reality, and the internet, the demand for huge information transfer and data rate with large capacity are increasing. The mm-wave spectrum band thus becomes the best choice for 5G networking applications. In the recent past, the researches mainly focus on the 28 GHz and 60 GHz [1] band which are allotted by the FCC for 5G communication application and millimeter wave (mm-Wave) component such as filter, coupler, and antenna. Due to high path loss and attenuation of the electromagnetic (EM) waves at mm-Wave spectrum, the Signal-To-Interference-Plus-Noise Ratio (SINR) will decrease. This is the major drawback of the mm-wave spectrum, which can be overcome by implementation of MIMO.

MIMO technology is a spatial domain technique which makes use of multiple transmitting and receiving antennas to enhance all the key requirements of the communication systems such as capacity of the channel, data rate, and reliability [2, 3]. When more than one antenna is placed close to each other, the major problem is the performance degradation due to low isolation between the elements. There are two approaches to increase the separation between the elements of the antenna. One is to reduce the field between the elements of the antenna [4], and the other is the use of networks of decoupling [5, 6].

The above-mentioned techniques give reasonable decoupling at microwave frequencies, but at mm-Wave spectrum direct scaling [7] is required which is difficult to obtain, and another major issue is decoupling elements losses. Therefore, there is a need for simple technique for decoupling with very low loss at mm-Wave spectrum.

Received 26 November 2019, Accepted 23 March 2020, Scheduled 31 March 2020

* Corresponding author: Nimmagadda Satyanarayana Murthy (nsmmit@gmail.com).

The author is with the ECE Department, V R Siddhartha Engineering College, Vijayawada, India.

2. LITERATURE SURVEY

With no surface wave generation and high efficiency, DRA has plenty of advantages to be operated at mm-Wave spectrum [8]. DRA based MIMO antennas have already been investigated [9,10]. It is reported that mm-Wave spectrum 28 GHz and 38 GHz band with bandwidth of 500 MHz could be used for 5G wireless communication systems [11]. Antenna arrays with high gain performance may be required to reduce the path loss in short range communication. When considering the multipath fading effect, the DRA built-in MIMO antenna will be good for the 5G communication application. In [12] a 9×9 MIMO antenna is proposed for 5G application, with the help of an external decoupling structure, and the isolation is improved. In [13], a Yagi-uda antenna with dual polarizations is proposed for 5G communication, and an external decoupling structure is used to increase the isolation performance.

For mm-Wave 5G cellular handsets working in the 28 GHz band, a DRA is suggested in [14]. In [15], with the help of corrugated metamaterial surface the isolation is improved, but the radiation pattern is not stable, and similarly in [16], a 4×4 MIMO antenna is proposed for 5G communication application. In [17], applications for 4G Long Term Evolution (LTE) and mm-Wave 5G are proposed for corner bent MIMO antennas. A MIMO mm-Wave antenna operating at 24 GHz is proposed in [18], which is ideal for wearable applications. In [19], a dual-polarized broadband horn antenna for mm-Wave 5G application and in [20], a MIMO DRA with enhanced isolation with the help of metal strips are proposed. In all the proposed work in the literature, the isolation is improved with the help of external decoupling structures. As a result, the size and fabrication become the main constraint in the design of antenna for 5G communication.

The structure of the paper is depicted as follows. Section 3 describes Proposed Meta-material MIMO DRA Design. Sections 4 and 5 explain the parametric analysis of the critical parameters, and metamaterial extraction procedure is presented. The outcome is addressed in Section 6 in order to confirm the suggested antenna. Finally, the conclusion is provided in Section 7.

3. PROPOSED META-MATERIAL MIMO DRA DESIGN

Figure 1 and Table 1 reflect the structure and its metamaterial-inspired MIMO DRA parameter. The planned MIMO DRA as a whole has a total dimension of $20 \text{ mm} \times 40 \text{ mm} \times 1.6 \text{ mm}$. The material used for the substrate is FR4, and the dielectric resonators are made of RO5880 material with a permittivity of 9.8 and loss of $\tan 0.0009$, and thickness of the dielectric material is 1.6 mm. A four-element antenna is proposed with four DRs, and each DR is excited with the help of a microstrip fed rectangular slot of length f and width h . On the top of each DRA, a metamaterial structure is printed in order to improve the isolation performance.

Table 1. Parameters values of the 4 element MIMO DRA (in mm).

w	L	$l1$	a	b	c	d
20	40	8.8	12.2	4.3	1.4	7.5
e	f	g	h	i	j	k
9.5	2.7	7	0.6	5.95	0.6	1.6

Four identical rectangular dielectric resonators made up of RO5880 with permittivity equal to 9.8 and loss $\tan 0.0009$ with $7.5 \text{ mm} \times 9.5 \text{ mm} \times 1.6 \text{ mm}$ dimension are placed on top of the microstrip fed slot. The proposed structure has very good return loss with the maximum value of -46.20 dB . The bandwidth of the proposed antenna is 2.85 GHz with the operating frequency range from 26.64 GHz to 29.50 GHz. The isolation of the proposed structure is about -15.2 dB . In order to improve the isolation performance of the proposed four elements MIMO DRA, a metamaterial structure is printed on top of the dielectric resonator.

In Figure 2, the s parameter plots with and without metamaterial are presented, from which we can clearly observe that with the inclusion of the metamaterial structure the isolation is improved with 2 dB as minimum value and 13 dB as maximum value. The metamaterial inclusion does not have much

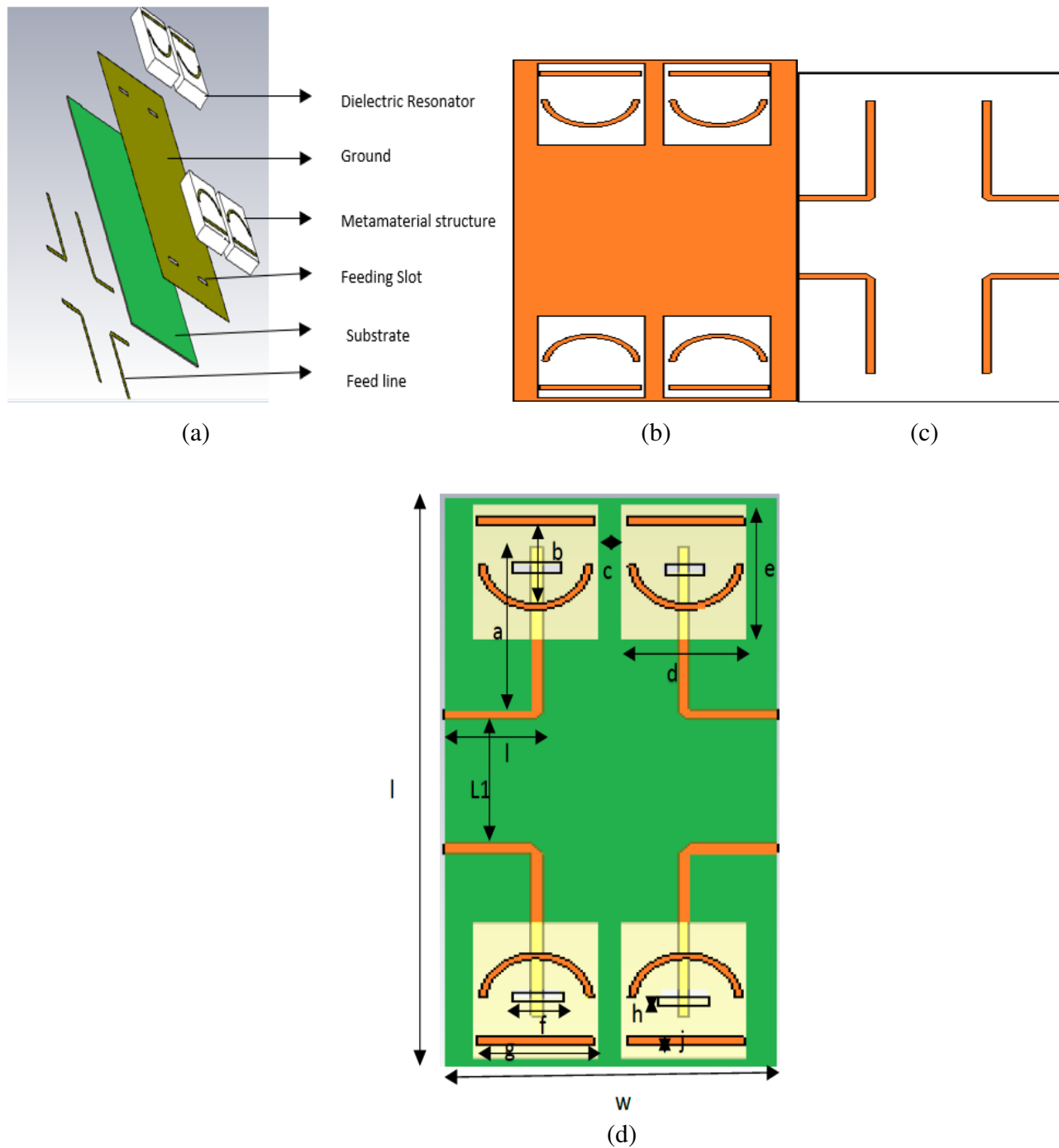


Figure 1. Proposed 4 element MIMO DRA antenna. (a) 3D analysis of the proposed 4 element MIMO DRA, (b) top view, (c) bottom view, (d) geometry and its parameters.

effect on bandwidth and return loss. The simulated result of the proposed 4 element MIMO DRA with and without metamaterial is presented in Table 2.

In Figure 3 and Figure 4, the return loss plot and VSWR of the proposed four element antenna depict good return loss, which shows that it has good impedance matching. The VSWR for each port is maintained below 2 in the entire band of operation. The rectangular DRA radiates like a short magnetic dipole, and it supports transverse electric modes $TE_{\delta 11}^x$.

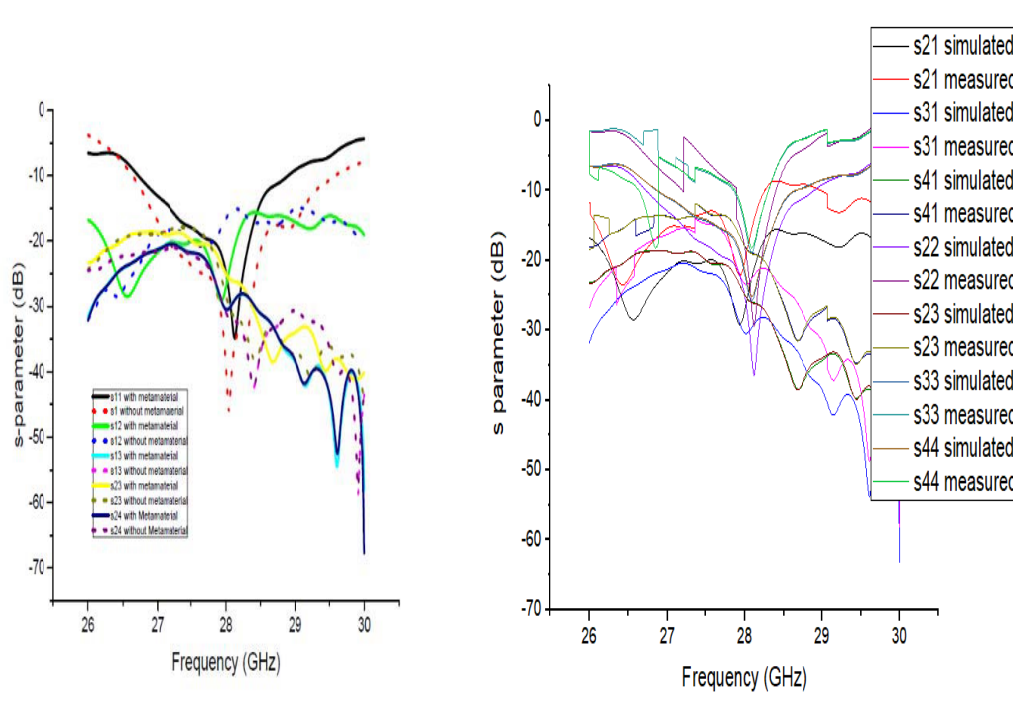


Figure 2. S parameter with and without metamaterial (simulated and measured).

Table 2. Comparison of proposed 4 element MIMO DRA with and without metamaterial.

Proposed antenna	Operating frequency range	Bandwidth	Return loss	Isolation
With metamaterial	26.71 GHz–28.91 GHz	2.20 GHz	–35 dB	–29.34 dB
Without metamaterial	26.61 GHz–29.57 GHz	2.59 GHz	–46.52 dB	–16.07 dB

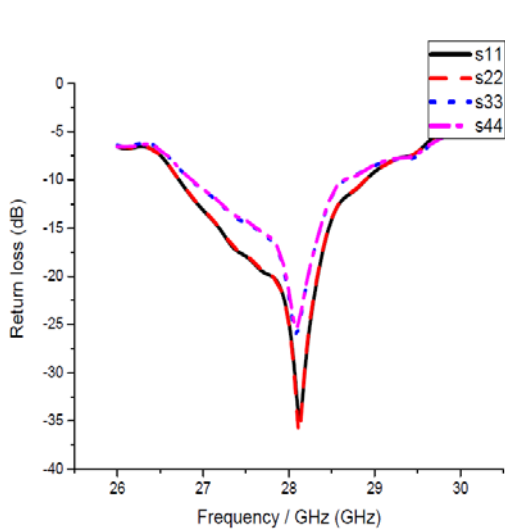


Figure 3. Return loss plot (each port excited).

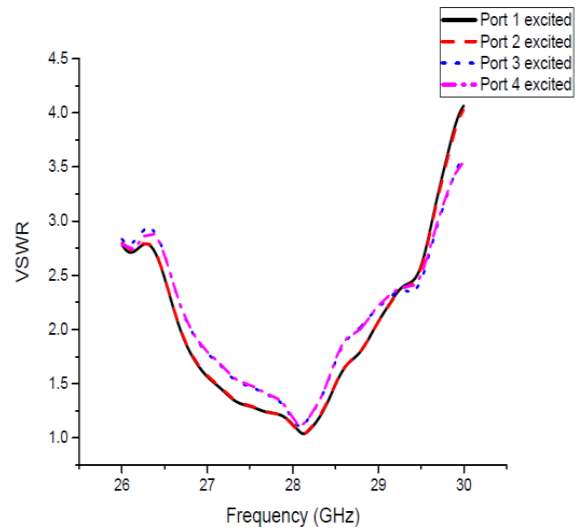


Figure 4. VSWR plot (each port excited).

The resonant frequency of a rectangular DRA for TE_{abc}^y mode can be extracted from the wave numbers k_a , k_b , and k_c within the DRA, and the subscriptions a — number of standing waves along the x -axis, b — number of standing waves along the y -axis, and c — number of standing waves along the z -axis, determined from [24].

The maximum part of the field coupling is exactly above the slot which can be easily coupled to port 2 via the slot available in the ground. After the inclusion of the metamaterial in the upper part of the dielectric resonator, the coupling fields are not on top of the slots. In this way, the coupling field is reduced which leads to the improvement of isolation performance. In Figure 5, the isolation performance of the proposed 4 element metamaterial inspired MIMO DRA is presented from which we can clearly infer that the isolation performance is very good for the proposed antenna, as all the isolation values are well maintained below -20 dB in the entire band of operation.

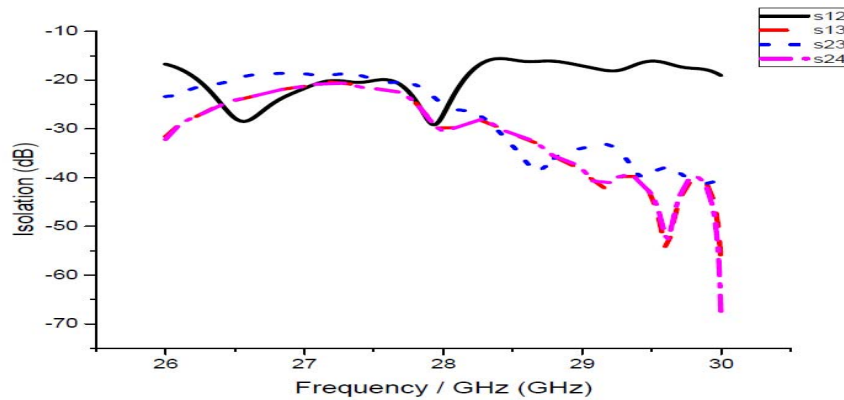
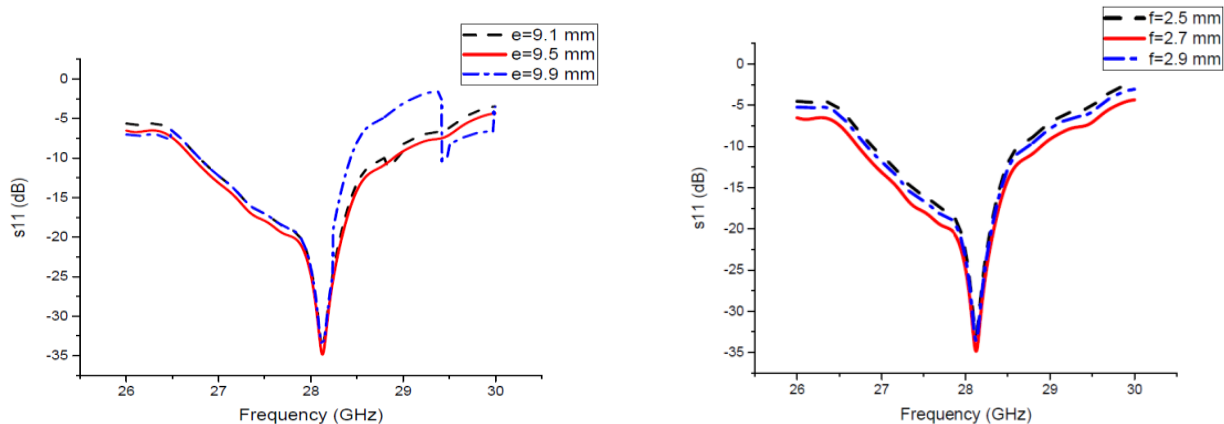


Figure 5. Isolation plot (each port excited).

4. PARAMETRIC ANALYSIS

The parametric study of return loss is shown in Figure 6. Such parameters are DRA width (e), slot length (f), and slot width (h). The width of the DRA in steps of 0.4 mm ranges from 9.1 mm to 9.9 mm, and it is clearly observed that $e = 9.5$ mm is capable of achieving reasonable bandwidth, so it is chosen as the optimum value. Then the width of the slot is considered for parametric analysis, and its value is varied from 0.4 mm to 0.8 mm. The width of the slot at $h = 0.6$ mm has good impedance bandwidth along with matching, and hence it is chosen as optimum value. Similarly, the length of the slot is varied in steps of 0.2 mm from 2.5 mm to 2.9 mm, and 2.7 mm is chosen as the optimum value, since it can achieve good impedance matching.



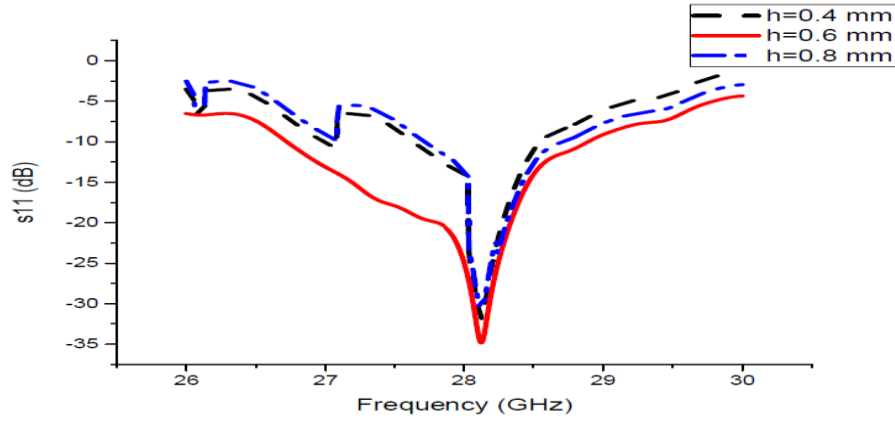


Figure 6. Parametric analysis of proposed MIMO DRA.

From the analysis of parametric study regarding slot, its length f and width h variations play a vital role in matching the power from aperture coupled technique. As the values of these dimensions vary, the port power gets mismatched causing the impedance to vary from standard value of 50 ohms, resulting in reduced bandwidth. As the width of DRA is varied, the upper cutoff frequency decreases slightly thereby reducing the impedance bandwidth.

5. EXTRACTION OF META-MATERIAL PROPERTY

CST Software is used to model materials in rectangular waveguide environments for the measurement of S -parameters (S_{11} and S_{21}) from which the constituent parameters can be extracted. The negative permeability of Split Ring Resonator (SRR) and permittivity of Complementary SRR are extracted with the help of Nicolson-Ross-Weir (NRW) method

$$V_1 = S_{21} + S_{11} \quad (1)$$

$$V_2 = S_{21} - S_{11} \quad (2)$$

$$S_{11} = \text{re}(S_{11}) + j(\text{im}(S_{11})) \quad (3)$$

$$S_{21} = \text{re}(S_{21}) + j(\text{im}(S_{21})) \quad (4)$$

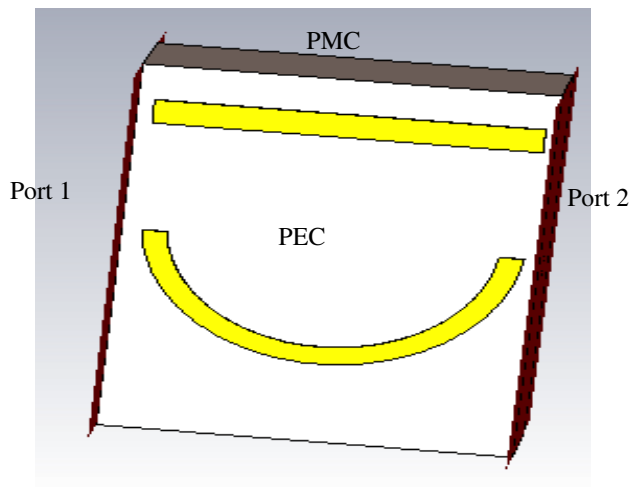


Figure 7. Waveguide extraction method for retrieving S_{11} and S_{21} .

$$\mu = \frac{2}{jK_O d} * \frac{1 - V_2}{1 + V_2} \tag{5}$$

$$\varepsilon = \frac{2}{jK_O d} * \frac{1 - V_1}{1 + V_1} \tag{6}$$

where d is a thickness of the substrate, and K_O is a wave number. Using CST Microwave Studio, the waveguide extraction, shown in Figure 7, with the help of MATLAB coding the negative permittivity, permeability, and refractive index of the proposed antenna is shown in Figure 8.

6. RESULT AND DISCUSSION

In Figure 9, the surface current density of the proposed antenna is depicted. It is observed that there are very few coupling fields between the elements because of the presence of metamaterial structure. The metamaterial structure can move the strongest coupling field between the elements. In this way, the isolation is improved.

Figure 10 shows the radiation pattern of the proposed 28 GHz antenna. The radiation reveals a clear omnidirectional pattern that is the core requirement for any communication application. The radiation pattern is not so much influenced by the metamaterial structure, since the metamaterial is

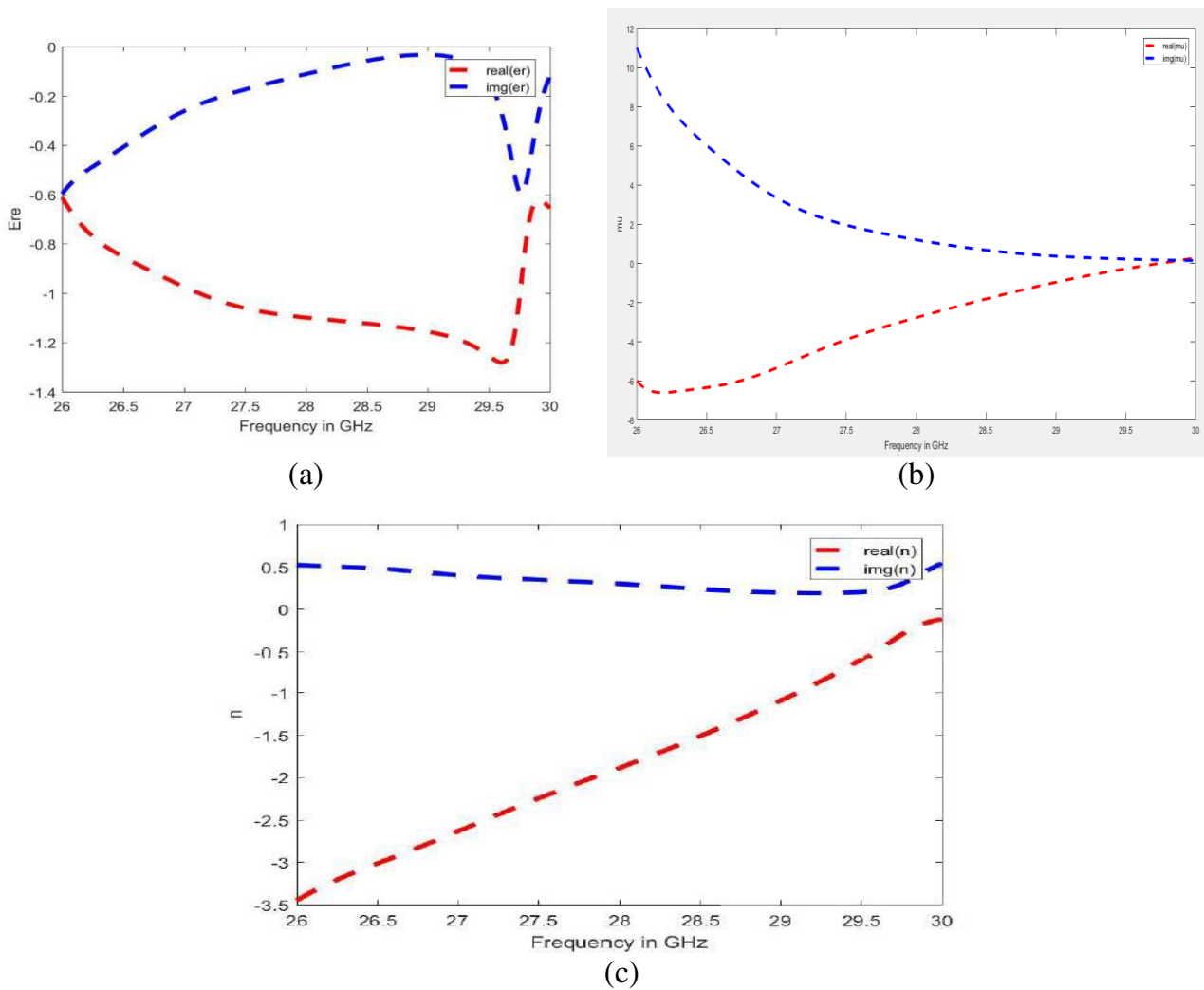


Figure 8. (a) Permittivity characteristics, (b) permeability characteristics, (c) refractive index.

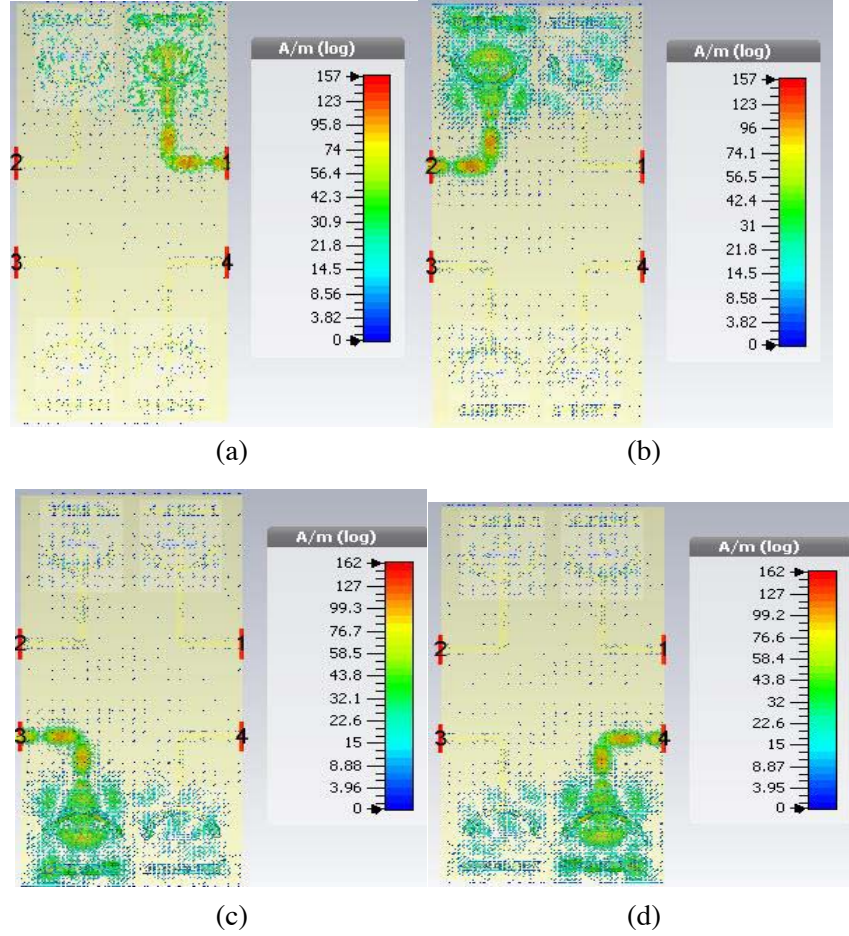


Figure 9. Surface current. (a) Port 1 excited, (b) port 2 excited, (c) port 3 excited, (d) port 4 excited.

printed on the dielectric resonators where the electrical field is very small. The 3D gain pattern is shown in Figure 11, and it has the highest directive gain perpendicular to the antenna axis.

From Figure 12, it is observed that the radiation efficiency is above 88% in the entire operating band from 26.71 GHz to 28.91 GHz. From Figure 13, it is shown that the gain is above 7.5 dBi in the entire operating band from 26.71 GHz to 28.91 GHz.

The efficiency of the MIMO antenna is calculated using the antenna diversity metric. This work uses the technique of spatial diversity to realize the antenna diversity and to improve the distinction between two closely coupled antennas. ECC is used to determine the separation between two closely coupled antennas and can be measured using far-field patterns. When the ECC value is lower than the efficiency of the MIMO antenna diversity is strong. The method for determining the coefficient of association between antennas i and j in an antenna system with N -element MIMO is

$$\rho_e(i, j, N) = \left| \frac{\sum_{n=1}^N S_{i,n}^* S_{n,j}}{\prod_{k=i,j} \left(1 - \sum_{n=1}^N S_{k,n}^* S_{n,j} \right)} \right| \quad (7)$$

For two element MIMO:

$$\rho_e(1, 2, 2) = \frac{|S_{11}^* S_{12} + S_{21}^* S_{22}|^2}{(1 - |S_{11}|^2 - |S_{21}|^2)(1 - |S_{22}|^2 - |S_{12}|^2)} \quad (8)$$

For four element MIMO:

$$\rho_e(1, 2, 4) = \frac{|S_{11}^* S_{12} + S_{21}^* S_{22} + S_{13}^* S_{32} + S_{14}^* S_{42}|^2}{(1 - |S_{11}|^2 - |S_{21}|^2 - |S_{31}|^2 - |S_{41}|^2)(1 - |S_{12}|^2 - |S_{22}|^2 - |S_{32}|^2 - |S_{42}|^2)} \quad (9)$$

$$\rho_e(1, 3, 4) = \frac{|S_{11}^* S_{13} + S_{21}^* S_{23} + S_{13}^* S_{33} + S_{14}^* S_{43}|^2}{(1 - |S_{11}|^2 - |S_{21}|^2 - |S_{31}|^2 - |S_{41}|^2)(1 - |S_{13}|^2 - |S_{23}|^2 - |S_{33}|^2 - |S_{43}|^2)} \quad (10)$$

From [21], it is noted that the ECC based on the far field is the correct method to find the ECC. So, with the help of CST software the ECC based on far field is presented in Figure 14. In Figure 14, the simulated envelope correlation coefficient is presented, which clearly depicts that the ECC value is well below 0.05 in the entire operating band, and diversity gain is plotted in Figure 15 with the help of the following equation.

$$DG = 10p \quad (11)$$

$$p = (1 - |0.99e|^2)^{1/2} \quad (12)$$

where

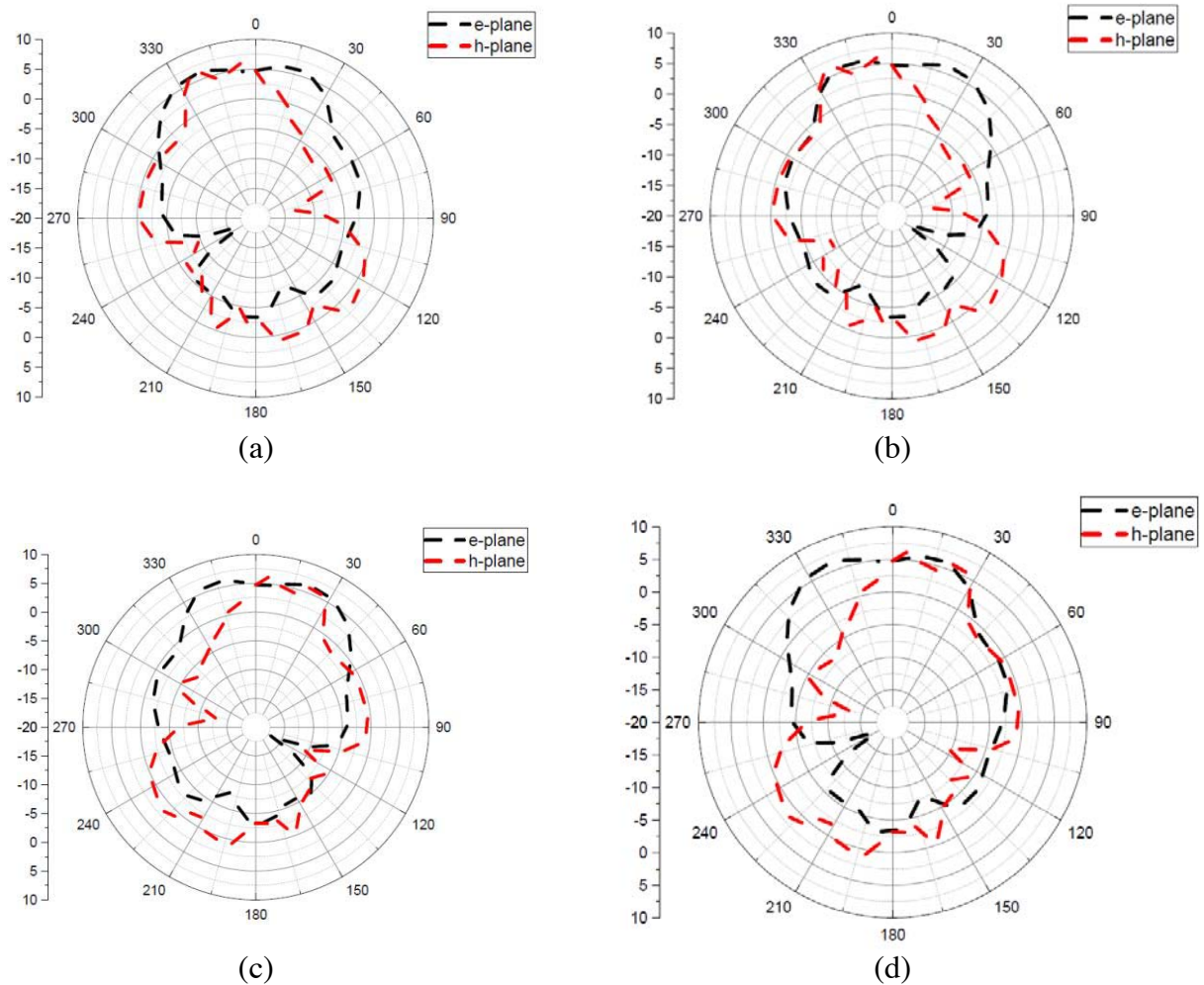


Figure 10. Radiation pattern. (a) Port 1 excited, (b) port 2 excited, (c) port 3 excited, (d) port 4 excited.

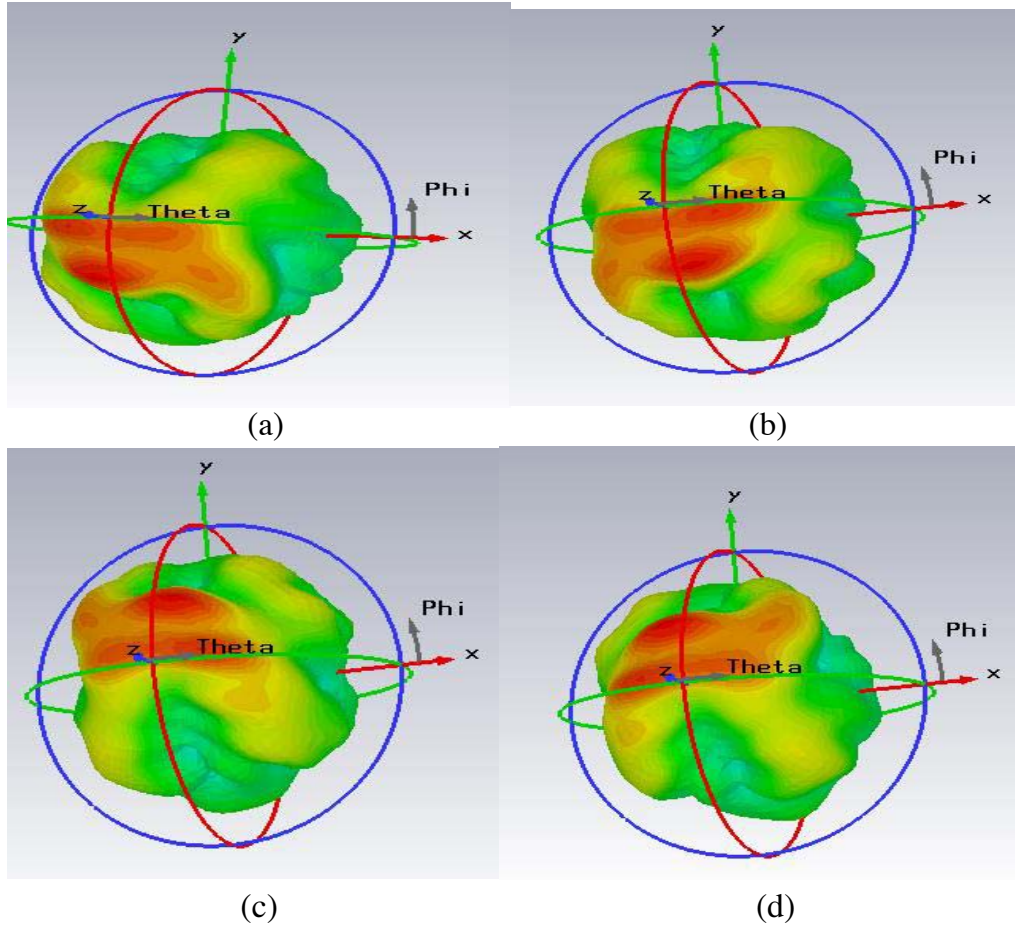


Figure 11. 3D gain pattern. (a) Port 1 excited, (b) port 2 excited, (c) port 3 excited, (d) port 4 excited.

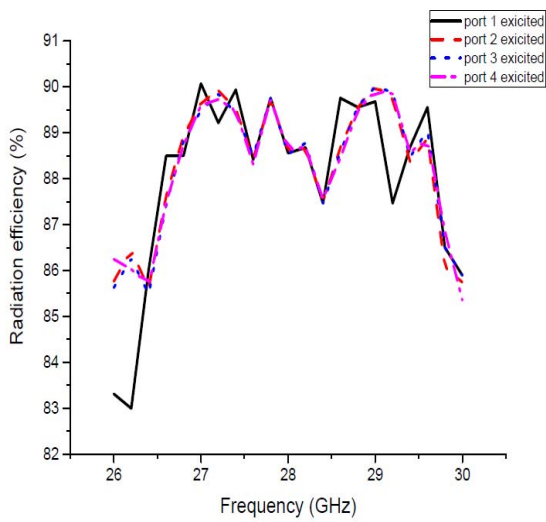


Figure 12. Radiation efficiency.

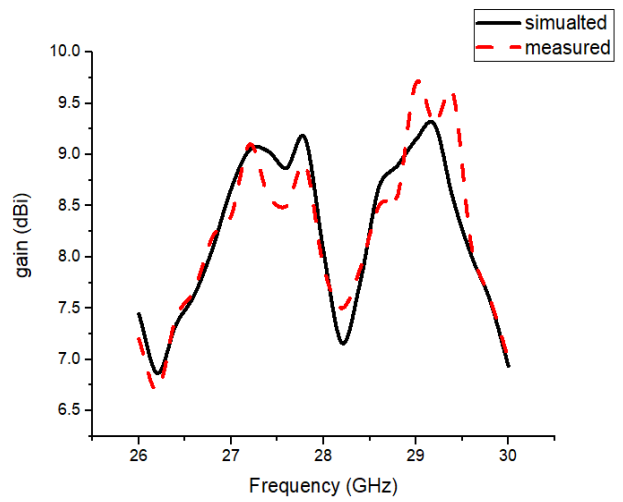


Figure 13. Gain of the proposed MIMO DRA.

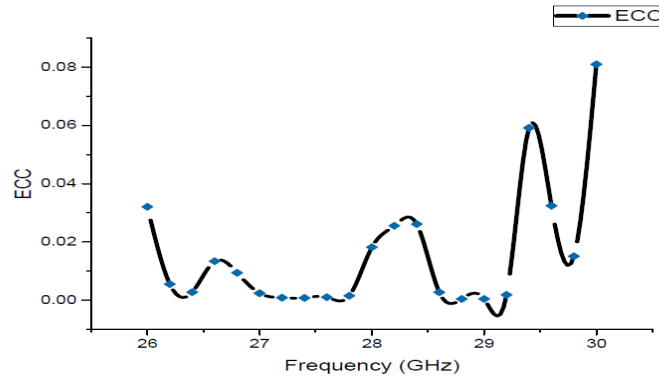


Figure 14. ECC of the proposed MIMO DRA (based on farfield pattern simulated using CST).

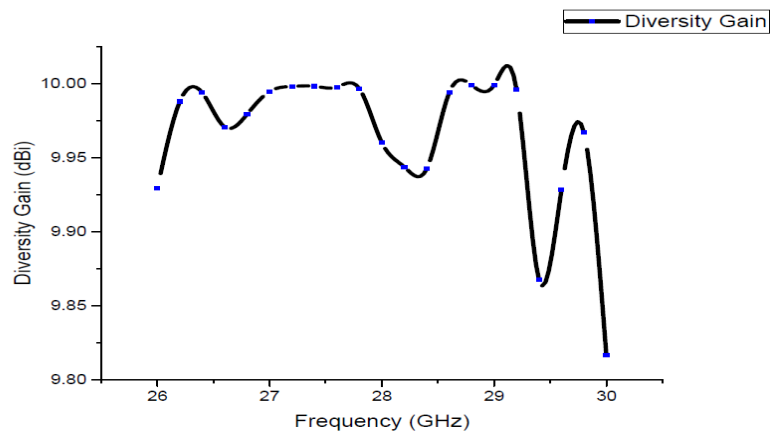


Figure 15. Diversity gain of the proposed MIMO DRA.

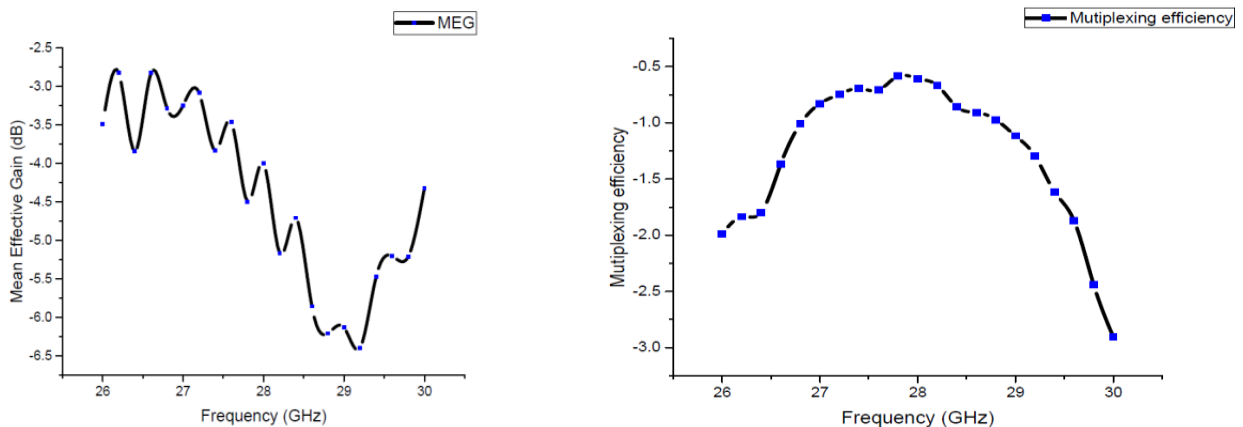


Figure 16. MEG and multiplexing efficiency of the proposed MIMO DRA.

10 is the maximum DG with selection combining probability level 1%

ρ is the correlation efficiency approximate expression

It is observed from Figure 15 that the diversity gain in the entire operating band is above 9.90 dBi from 26.71 GHz to 28.91 GHz. Figure 16 shows the mean efficient gain and multiplexing efficiency in terms of frequency, clearly with peak mean effective gain (MEG) value of -4 dB and -1 dB multiplexing

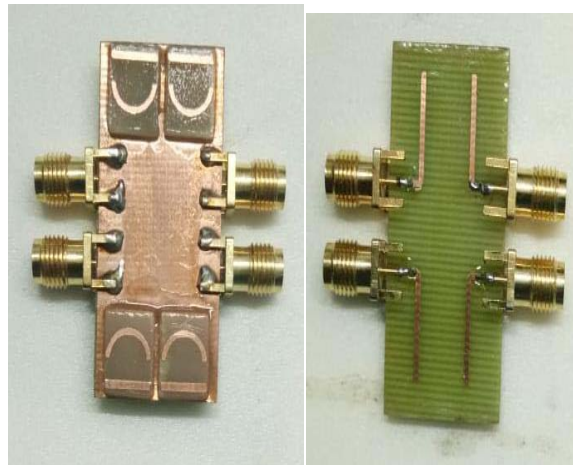
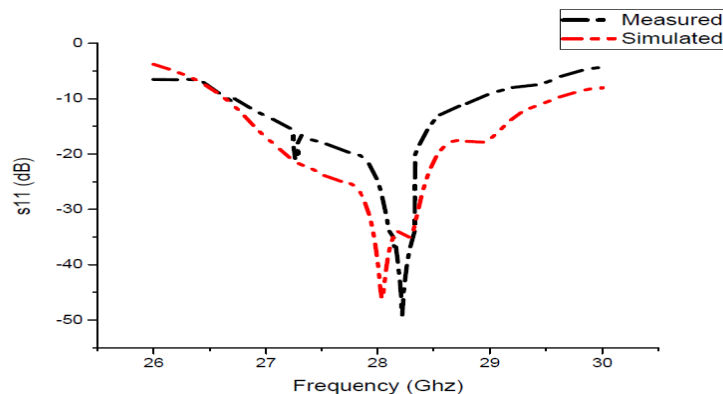
Table 3. Proposed work vs counterparts.

Ref. no	Total size	No. of ports	Operating band	isolation
12	48 mm × 21 mm	2	29.7 GHz to 31.5 GHz	25 dB
13	128 mm × 31 mm	4	31 GHz to 40.3 GHz	21 dB
14	42 mm × 85 mm	2	27 GHz to 32 GHz	37 dB
15	48 mm × 31 mm	4	26 GHz to 31 GHz	21 dB
Proposed method	20 mm × 40 mm	4	26.71 GHz to 28.91 GHz	29.34 dB

efficiency in the 28 GHz operating band.

A dual-band cylindrical dielectric resonator antenna is proposed in [22], in which the miniaturization and dual-band frequency activity are accomplished by loading circular copper strips on top of the CDA with a maximum gain of 5.6 dBi. As a method of miniaturization, a square dielectric resonator is fitted with a magnetic LC resonator. It has dual-band operation and a maximum gain of 6 dBi at 35 GHz [23]. However in our proposed work, with the help of metamaterial 2.20 GHz impedance bandwidth with gain above 7 dBi is achieved, and the metamaterial property is verified. The proposed scheme and existing methods of MIMO DRA with improved isolation are presented in Table 3.

In Figure 17, the front view and back view of the fabricated antenna are shown, and in Figure 18,

**Figure 17.** Front and back view of the fabricated proposed MIMO DRA.**Figure 18.** Measured vs simulated return loss plot of the proposed MIMO DRA.

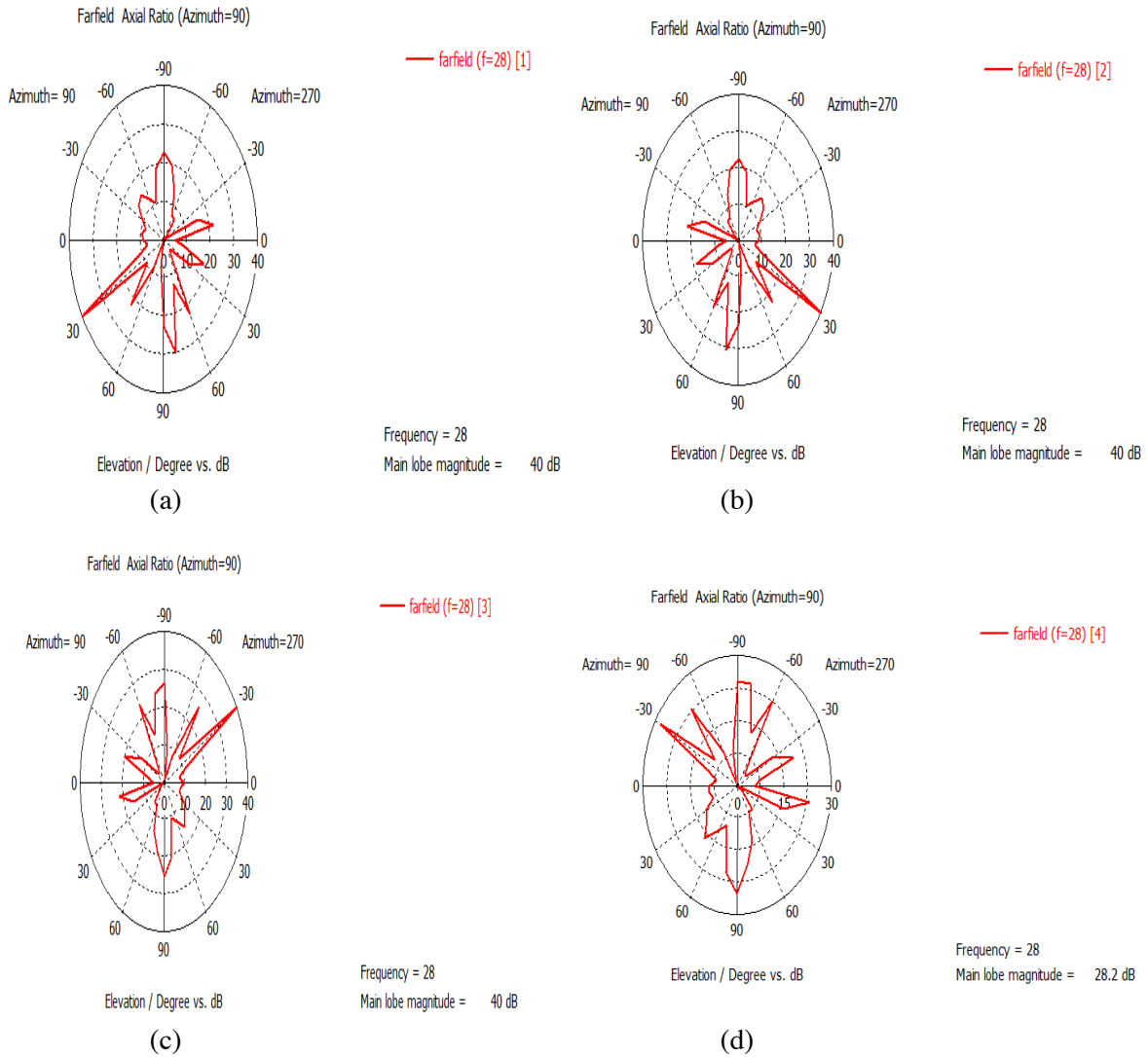


Figure 19. Axial ratio plot of the proposed MIMO DRA. (a) Port 1 excited, (b) port 2 excited, (c) port 3 excited, (d) port 4 excited.

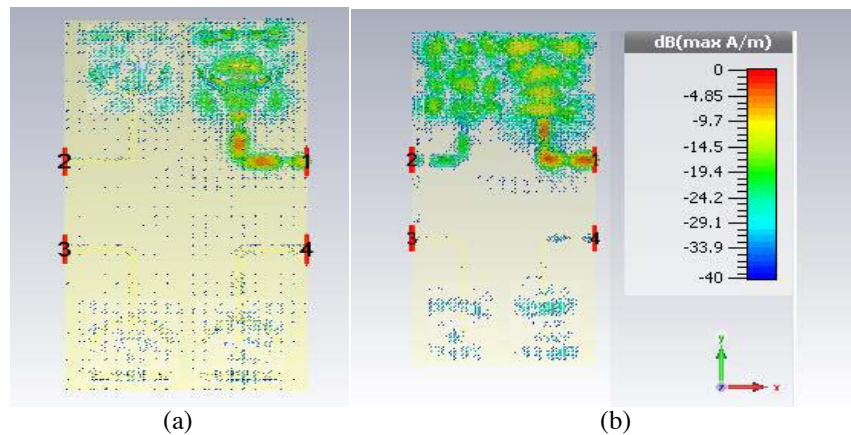


Figure 20. Surface current distribution (dBmax) when port 1 is excited. (a) With metamaterial, (b) without metamaterial.

the measured vs simulated return loss plot is depicted which clearly shows that there is a little deviation between the results which is due to fabrication and connector errors.

In Figure 19, the axial ratio of the proposed antenna is presented. From Figure 20, we can clearly see that the coupling field is more when the metamaterial is not available in the design. The metamaterial decouples the coupling field effect. The figure represents the surface current distributions with and without the metamaterial.

7. CONCLUSION

For the next generation 5G antenna, a 4×4 MIMO DRA antenna is suggested. It is mounted on a $20 \text{ mm} \times 40 \text{ mm}$ FR4 substrate. Four dielectric resonators are mounted above the slotted ground plane with aperture coupled feeding. This device resonates from 26.6 GHz to 29.57 GHz at 28 GHz band, with isolation of -16.07 dB . With the aid of the novel metamaterial structure, which is printed on top of the four dielectric resonators finished up with Roger 5880, the insulation is improved. The metamaterial structure is capable of decoupling the fields between the closely coupled antenna elements without affecting the radiation pattern, since the structure is printed on the weak electric field area of the dielectric resonator. This system has an operating frequency range of 26.71 GHz to 28.91 GHz with maximum -29.34 dB isolation. By including the metamaterial structure, the isolation is improved which is a key parameter in MIMO. The metamaterial property is also extracted using waveguide method. All the simulated results are presented with the help of CST software. The small deviation between the measured and simulated results is due to the manufacturing and measuring errors. Because of its lowest ECC value, stable radiation pattern and high gain, the proposed MIMO DRA antenna is an accurate option for future generation 5G communication.

REFERENCES

1. Niu, Y., Y. Li, D. Jin, L. Su, and A. V. Vasilakos, "A survey of millimeter wave (mmWave) communications for 5G: Opportunities and challenges," *Wireless Networks*, Vol. 21, No. 8, 2015.
2. Hong, W., "Solving the 5G mobile antenna puzzle: Assessing future directions for the 5G mobile antenna paradigm shift," *IEEE Microwave Magazine*, Vol. 18, No. 7, 86–102, Nov.–Dec. 2017.
3. Hong, W., et al., "Multibeam antenna technologies for 5G wireless communications," *IEEE Trans. Antennas Propag.*, Vol. 65, No. 12, 6231–6249, Dec. 2017.
4. Yang, X., Y. Liu, Y. X. Xu, and S. X. Gong, "Isolation enhancement in patch antenna array with fractal UC-EBG structure and cross slot," *IEEE Antennas Wireless Propag. Lett.*, Vol. 16, 2175–2178, 2017.
5. Wu, C. H., C. L. Chiu, and T. G. Ma, "Very compact fully lumped decoupling network for a coupled two-element array," *IEEE Antennas Wireless Propag. Lett.*, Vol. 15, 158–161, 2016.
6. Zhang, S. and G. F. Pedersen, "Mutual coupling reduction for UWB MIMO antennas with a wideband neutralization line," *IEEE Antennas Wireless Propag. Lett.*, Vol. 15, 166–169, 2016.
7. Farahani, H. S., M. Veysi, M. Kamyab, and A. Tadjalli, "Mutual coupling reduction in patch antenna arrays using a UC-EBG superstrate," *IEEE Antennas Wireless Propag. Lett.*, Vol. 9, 57–59, 2010.
8. Petosa, A., *Dielectric Resonator Antenna Handbook*, 1st Edition, Artech House, Boston, 2007.
9. Hussain, M. T., O. Hammi, M. S. Sharawi, S. K. Podilchak, and Y. M. M. Antar, "A dielectric resonator based millimeter-wave MIMO antenna array for hand-held devices," *2015 IEEE International Symposium on Antennas and Propagation USNC/URSI National Radio Science Meeting*, 3–4, Jul. 2015.
10. Hussain, M. T., M. S. Sharawi, S. Podilchack, and Y. M. M. Antar, "Closely packed millimeter-wave MIMO antenna arrays with dielectric resonator elements," *2016 10th European Conference on Antennas and Propagation (EuCAP)*, 1–4, Apr. 2016.
11. Sharawi, M. S., "Printed multi-band MIMO antenna systems and their performance metrics [wireless corner]," *IEEE Antennas and Propagation Magazine*, Vol. 55, No. 5, 218–232, Oct. 2013.

12. Sharawi, M. S., S. K. Podilchak, M. T. Hussain, and Y. M. M. Antar, "Dielectric resonator based MIMO antenna system enabling millimetre-wave mobile devices," *IET Microwaves, Antennas & Propagation*, Vol. 11, No. 2, 287–293, 2017.
13. Hsu, Y. W., T. C. Huang, H. S. Lin, and Y. C. Lin, "Dual polarized quasi Yagi-Uda antennas with endfire radiation for millimeter-wave MIMO terminals," *IEEE Trans. Antennas Propag.*, Vol. 65, No. 12, 6282–6289, 2017.
14. Wang, H., "Quasi-Yagi antenna array with modified folded dipole driver for mmWave 5G cellular devices," *IEEE Antennas Wireless Propag. Lett.*, Vol. 18, No. 5, 971–975, Jun. 2019.
15. Gupta, S., et al., "Mutual coupling reduction using metasurface corrugations for 28 GHz MIMO applications," *IEEE Antennas Wireless Propag. Lett.*, Vol. 16, 2763–2766, 2017.
16. Wani, Z., M. P. Abegaonkar, and S. K. Koul, "A 28-GHz antenna for 5G MIMO applications," *Progress In Electromagnetics Research Letters*, Vol. 78, 73–79, 2018.
17. Idrees Magray, M., G. S. Karthikeya, K. Muzaffar, and S. K. Koul, "Corner bent integrated design of 4G LTE and mmWave 5G antennas for mobile terminals," *Progress In Electromagnetics Research M*, Vol. 84, 167–175, 2019.
18. Iqbal, A., A. Basir, A. Smida, N. K. Mallat, I. Elfergani, J. Rodriguez, and S. Kim, "Electromagnetic bandgap backed millimeter-wave MIMO antenna for wearable applications," *IEEE Access*, Vol. 7, 111135–111144, 2019.
19. Hu, N., W. Xie, Q. Zeng, J. Liu, L. Zhao, and S. Liu, "A dual-polarized broadband horn antenna for mm-wave 5G application," *2019 Cross Strait Quad-Regional Radio Science and Wireless Technology Conference (CSQRWC)*, 1–2, IEEE, 2019.
20. Zhang, Y., J. Y. Deng, M. J. Li, D. Sun, and L. X. Guo, "A MIMO dielectric resonator antenna with improved isolation for 5G mm-wave applications," *IEEE Antennas Wireless Propag. Lett.*, Vol. 18, No. 4, 747–751, Feb. 2019.
21. Sharawi, M. S., "Current misuses and future prospects for printed multiple-input, multiple-output antenna systems [wireless corner]," *IEEE Antennas and Propagation Magazine*, Vol. 59, No. 2, 162–170, Apr. 2017.
22. Iqbal, A., A. Bouazizi, S. Kundu, I. Elfergani, and J. Rodriguez, "Dielectric resonator antenna with top loaded parasitic strip elements for dual-band operation," *Microw. Opt. Technol. Lett.*, Vol. 61, 2134–2140, 2019.
23. Sharma, A., A. Sarkar, A. Biswas, and M. Jaleel Akhtar, "Compact dual-band hybrid dielectric resonator antenna loaded with magnetic-LC resonator," *Journal of Electromagnetic Waves and Applications*, Vol. 32, No. 6, 1298–1305, Jul. 3, 2018.
24. Mongia, R. K., "Theoretical and experimental resonant frequencies of rectangular dielectric resonators," *IEE Proceedings H — Microwaves, Antennas and Propagation*, Vol. 139, No. 1, 98–104, 1992.